Neurovascular-modulation

Niranjan Khadka, Marom Bikson
Department of Biomedical Engineering, The City College of New York, CUNY, New York, NY, 10031

Correspondence

Marom Bikson
Tel: (212) 650- 7076
email: bikson@ccny.cuny.edu

Niranjan Khadka
Tel: (212) 650- 7076
email: nironzan@gmail.com

Acknowledgments

Source(s) of financial support: This study was partially funded by grants to MB from NIH (NIMH 1R01MH111896, NINDS 1R01NS101362, NCI U54CA137788/ U54CA132378, R03 NS054783, 1R01NS112996-01A1) New York State Department of Health (NYS DOH, DOH01-C31291GG), and cycle 50 PSC-CUNY.

Conflict of Interest

The City University of New York (CUNY) has IP on neuro-stimulation systems and methods with authors NK and MB as inventors. MB has equity in Soterix Medical. MB served on the advisory boards, received grants, and/or consulted for Boston Scientific, Mecta, Halo Neuroscience, and GlaxoSmithKline Inc.

Abstract

Neurovascular-modulation is based on two principles that derive directly from brain vascular ultra-structure, namely an exceptionally dense capillary bed (BBB length density: 972 mm/mm^3) and a blood-brain-barrier (BBB) resistivity (ρ ~ 1x10^5 Ω.m) much higher than brain parenchyma/interstitial space (ρ ~ 4 Ω.m) or blood (ρ ~ 1 Ω.m). Principle 1: Electrical current crosses between the brain parenchyma (interstitial space) and vasculature, producing BBB electric fields (E_{BBB}) that are > 400x of the average parenchyma electric field ($\bar{E}_{BRAIN}$), which in turn modulates transport across the BBB. Specifically, for a BBB space constant (λ_{BBB}) and wall thickness ($d_{th\text{-}BBB}$): analytical solution for maximum BBB electric field (E^A_{BBB}) is given as: ($\bar{E}_{BRAIN}$ x λ_{BBB}) / $d_{th\text{-}BBB}$. Direct vascular stimulation suggests novel therapeutic strategies such as boosting metabolic capacity or interstitial fluid clearance. Boosting metabolic capacity impacts all forms of neuromodulation, including those applying intensive stimulation or driving neuroplasticity. Boosting interstitial fluid clearance has broad implications as a treatment for neurodegenerative disease including Alzheimer's disease. Principle 2: Electrical current in the brain parenchyma is distorted around brain vasculature, amplifying neuronal polarization. Specifically, vascular ultra-structure produces ~50% modulation of the average parenchyma electric field ($\bar{E}_{BRAIN}$) over the ~40 μm inter-capillary distance. The divergence of E_{BRAIN} (activating function) is thus ~100 kV/m^2 per unit average parenchyma electric field ($\bar{E}_{BRAIN}$). This impacts all forms of neuromodulation, including Deep Brain Stimulation (DBS), Spinal Cord Stimulation (SCS), Transcranial Magnetic Stimulation (TMS), Electroconvulsive Therapy (ECT), and transcranial electrical stimulation (tES) techniques such a transcranial Direct Current Stimulation (tDCS). Specifically, whereas spatial profile of E_{BRAIN} along neurons is traditionally assumed to depend on macroscopic anatomy, it instead depends on local vascular ultra-structure.

Introduction

Vascular responses are ubiquitous across neuromodulation [1–6], but are considered epiphenomena to neuronal stimulation. Common functional imaging techniques measure hemodynamic response (e.g. Arterial Spin Labeling fMRI, H_20^{15} PET, SPECT, BOLD fMRI, fNIRS) are interpreted as indexing neuronal activation through neurovascular coupling (NVC). Neurovascular coupling is the mechanism by which increased neuronal activity regulates cerebral blood flow (CBF) to assure that the blood supply of the brain is commensurate to local cellular metabolism [7,8]. The mechanisms of neurovascular coupling are studied to: enhance interpretation of hemodynamic-based imaging techniques [9]; and understand the role of cerebral blood flow and in disease such as hypertension, Alzheimer disease, and stroke [7]. Neurovascular coupling is activated in animals using mechanosensory stimulation [9–11], visual stimulation [12–14], and electrical stimulation of peripheral [15,16] or central axons *distal* to the brain region of interest [17–19]. Stimulation applied directly to a brain region is a special case where brain vasculature can be directly activated [20–22] which: 1) reverses the typical recruitment order of neurovascular coupling, suggesting functional imaging in fact shows direct hemodynamic activation; and 2) resulting in peculiar (supra-physiological) neurovascular changes that suggest novel therapeutic strategies (e.g. metabolic capacity, interstitial clearance).

The brain capillary bed is a dense network of interconnected vessels formed by specialized endothelial cells. The blood-brain-barrier (BBB) is the interface between the blood and brain interstitial fluid. Endothelial cells are sealed together by tight junctions, resulting in an exceptionally resistive BBB. Capillary diameter in the brain is ~10 μm and the average intercapillary distance is ~40 μm [23,24], such that neuronal processes are < 20 μm from the nearest capillary [25]. Moreover, brain capillaries are encased in extracellular matrix proteins and surrounded by specialized neuronal processes and the perivascular end feet of astrocytic glia [26].

Here we consider two consequences of BBB ultra-structure in neuromodulation. First, to what extent does the BBB polarize as a consequence of current crossing between interstitial space and the blood (Principle 1)? Neurovascular coupling and interstitial fluid clearance governs brain health and can be compromised in disease [7]. For example Alzheimer's Disease (AD) is associated with build-up of misfolded proteins [27,28] and impaired clearance systems [29]. Generally, interstitial fluid clearance is compromised with age [30] which may be linked to the role of clearance during sleep [31]. Interventions enhancing clearance in the brain may treat diverse neurological disorders including of aging [28]. By predicting BBB polarization, Principle 2 provides a substrate for developing neurovascular modulation targeting brain clearance. For example, we proposed tDCS boosts interstitial fluid transport based on BBB electro-osmosis [21].

Second, current flow through the interstitial space is considered insensitive to cellular ultra-structure [32], which has importance consequences for predicting which neuronal elements are stimulated [33]. But, the role of capillaries in distorting current flow is addressed for the first time here (Principle 2). We specifically advance the theory that if microscopic electric field gradients (Activating Function) around neurons created by BBB ultra-structure is larger than that produced by macroscopic tissues changes [34–37], then neuronal stimulation is in fact predicted by the average local electric field [38,39] as convoluted by regional BBB properties. The consequences

of this analysis span all forms of brain stimulation including Deep Brain Stimulation (DBS), Spinal Cord Stimulation (SCS), Transcranial Magnetic Stimulation (TMS), Electroconvulsive Therapy (ECT), and transcranial electrical stimulation techniques (tES) such a transcranial Direct Current Stimulation (tDCS).

Methods

The anatomy of brain vasculature is intractably complex across scales, and current crossing the BBB can exits at neighboring locations or traverse broadly across vascular system, such that macroscopic anatomy may impact microscopic current flow. We overcome this by designing models (e.g. capillary orientation and capillary border boundary conditions) such that assessed variables (e.g. question being asked) were independent of exterior volume dimensions or capillary length. For electric field amplification at the BBB, the models address question regarding the maximum current density crossing the BBB for a given capillary morphology. We also adapt neuron cable theory [40–44] to develop an analytical solution for maximum BBB polarization sensitivity. For addressing neuron polarization amplification by vascular ultra-structure, parallel vessels (with no tortuosity, and region-specific inter-capillary distance) are a conservative model.

Model Construction and Solution Method

We developed a computer-aided design (CAD) model of BBB ultra-structure to first assess electric field amplification at the BBB (Principle 1) and neuron polarization amplification by vasculature (Principle 2). Different prototypical BBB morphologies were modelled as CAD files in SolidWorks (Dassault Systemes Corp., MA, USA) and imported into Simpleware (Synopsys Inc., CA, USA) to generate an adaptive tetrahedral mesh using a built-in voxel-based meshing algorithm. Mesh density was refined until additional model refinement produced less than 1 % difference in extracellular voltage at the BBB. The resulting model consisted of > 28 million, > 68 million, and > 41 tetrahedral elements for the three exemplary prototypical capillary morphologies: (morphology 1) Semi-circular loop (fixed curvature width) with semi-infinite orthogonal straight segments (Fig. 1A1); (morphology 2) Semi-circular loop (varied curvatures) with semi-infinite parallel straight segments (Fig. 1B1); (morphology 3) Semi-infinite straight tube with variant terminal conditions (Fig. 1C1), and > 38 million, > 29 million, > 45 million, > 68 million, and > 70 million for cortical (Fig. 2A1), white-matter (Fig. 2A2), subcortical (Fig. 2A3), lumbar white-matter (Fig. 2A4), and lumbar grey-matter (Fig. 2A5) vasculature models, respectively.

Normal current density was applied to the one surface of the brain voxel while the opposite surface of the brain voxel was grounded, with the remaining external boundaries insulated. For computation, we used 0.08 A/m^2 (corresponding to ~1 mA tDCS [38]), however all results were reported as normalized (i.e. per unit parenchyma electric field) by dividing results by the average ("bulk") parenchyma electric field ($\bar{E}_{BRAIN}$). This is the same as the uniform electric field produced in a model with homogenous resistivity (i.e. only brain parenchyma). Laplace equation ($\nabla\cdot(\sigma\nabla V) = 0$, where V is extracellular voltage and σ is electrical conductivity) was applied and solved as the field equation to determine the extracellular voltage distribution throughout the model. Three-dimensional (3D) extracellular voltage, electric field, and activating function were predicted in different capillary morphologies, and resulting BBB polarization length, BBB amplification factor, or neuronal polarization amplification by vascular ultrastructure were calculated.

Models of BBB Electric Field Amplification (Principle 1): Numerical Solutions

For electric field amplification at the BBB, we simulated three variations of capillary morphology 1 namely I, I_1, and I_2, with fixed curvature width (1000 μm), and varied wall thickness ($d_{th\text{-}BBB}$), lumen diameter (d_l) and brain voxel volume. In variation I, the $d_{th\text{-}BBB}$ was 10 μm, d_l was 100 μm, and brain voxel volume was 2.2×10^{12} μm^3. In variation I_1 and I_2, the $d_{th\text{-}BBB}$ was 1 μm and d_l was 10 μm, while the brain voxel volumes were 5.1×10^7 μm^3 and 1.1×10^8 μm^3, respectively. Unless otherwise mentioned, 2.2×10^{12} μm^3 was used as a standard brain voxel volume for the remaining capillary morphology models. Capillary morphology 2 included two morphological variations namely II and II_2. In both of these variations, the $d_{th\text{-}BBB}$ was 10 μm and d_l was 100 μm, whereas the curvature widths were 1000 μm and 200 μm respectively for variation II and II_2. Capillary morphology 3 included III and III_1 morphological variations with variant terminal conditions. In variation III, one terminal of a semi-infinite straight tube was open, whereas both terminals were sealed in variation III_1. The $d_{th\text{-}BBB}$ was 10 μm and d_l was 100 μm for both III and III_1 variations. The semi-circular loop of capillary morphology 1 and 2 or tapered end of capillary morphology 3 were oriented toward the energized surface the brain voxel. Capillary wall and lumen dimensions were based on cadaveric studies and imaging data [45–52].

Unless otherwise indicated, standard electrical resistivity (reciprocal of electrical conductivity) was assigned to each model domain as: capillary wall: 1×10^5 Ω.m; capillary lumen: 1.42 Ω.m; and brain parenchyma: 3.62 Ω.m. In some simulations, capillary wall resistivity was increased or decreased 100-fold.

Capillary morphology 1 was positioned at the middle of the brain voxel in such a way that boundaries of capillary wall and lumen at the terminating ends of the orthogonal straight segments were sealed. Capillary wall and lumen boundaries at the terminating ends of the semi-infinite parallel segments of capillary morphology 2 were open (ground). Capillary morphology 3 was also positioned at the middle of the brain voxel, and the capillary lumen domain was enclosed by the capillary wall domain, with 1 μm spacing between them. Together they formed a semi-infinite membrane.

The numerical maxima for BBB polarization length (BBB polarization per unit parenchyma electric field) is given as:

$$V_{BBB} / \bar{E}_{BRAIN} \quad (1)$$

where V_{BBB} is a predicted BBB polarization (V) and $\bar{E}_{BRAIN}$ is an average predicted parenchyma electric field (V/m). The numerically-computed average BBB electric field amplification (BBB electric field per unit parenchyma electric field) is expressed as:

$$E_{BBB} / \bar{E}_{BRAIN} \quad (2)$$

where E_{BBB} (V/m) is an average electric field across the capillary wall thickness, calculated as V_{BBB} per BBB thickness:

$$V_{BBB} / d_{th\text{-}BBB} \quad (3)$$

The punctate (maximal) BBB electric field amplification is expressed as:

$$E^*_{BBB} / \bar{E}_{BRAIN} \quad (4)$$

where E^*_{BBB} (V/m) is the maximum predicted BBB electric field within the capillary wall, noting the electric field inside the capillary wall can change across the wall depth.

Models of BBB Electric Field Amplification (Principle 1): Analytical Solutions

Analytical analysis of polarization of axon terminals in an electric field based on cable theory [43,44,53] shows the maximal polarization that can be experienced at a bent or terminating axon terminal as:

$$V_{TM} = EF \times \lambda_m \quad (5)$$

where V_{TM} is the change in axon terminal transmembrane potential, EF is the electric field around the terminal (V/m), and λ_m is the terminal space constant (m). λ_m is a function of only the axon membrane resistivity (r_m: Ω.m) and axon intracellular resistivity (r_i: Ω.m) as:

$$\lambda_m = (r_m / r_i)^{1/2} \quad (6)$$

This maximal axon terminal polarization sensitivity may be secondarily amplified by "active" sub-threshold active channels at the terminal [54] and trigger a supra-threshold action potential. A maximal "passive" neuronal sensitivity of λ_m still applies, including to more complex neuronal structures [40,55].

Our analytical model for BBB polarization adapts this same cable theory where we model the capillary wall (BBB) as analogous to a continuous extracellular membrane and we model the capillary lumen (blood) as analogous to the continuous intracellular compartment. The analytically derived maximal BBB polarization is therefore expressed as:

$$V^A_{BBB} = \bar{E}_{BRAIN} \times \lambda_{BBB} \quad (7)$$

where V^A_{BBB} is BBB polarization (V), $\bar{E}_{BRAIN}$ is an average parenchyma electric field (V/m), and λ_{BBB} is defined here as the BBB space constant (m). λ_{BBB} is a function of only the capillary wall (BBB) resistivity (r_{BBB}: Ω.m) and capillary lumen (blood) resistivity (r_{BLOOD}: Ω.m) as:

$$\lambda_{BBB} = (r_{BBB} / r_{BLOOD})^{1/2} \quad (8)$$

The analytical polarization length (V^A_{BBB} per unit $\bar{E}_{BRAIN}$) is thus λ_{BBB}. The maximal analytical BBB electric field is then expressed as:

$$E^A_{BBB} = V^A_{BBB} / d_{th\text{-}BBB} \quad (9)$$

The analytical maximal amplification factor (E^A_{BBB} per unit $\bar{E}_{BRAIN}$) is then estimated as:

$$\lambda_{BBB}/d_{th\text{-}BBB} \quad (10)$$

Blood vasculature structure and properties are not simply analogous to axons of neurons, so we use numerical FEM simulations of various exemplary capillary morphologies to test if our analytical solution predicts maximal BBB polarization and so also the maximal BBB electric field. While we designed the models such that the V_{BBB} and E_{BBB} were independent of brain voxel size, anomalous current patterns where blood vessel contacting model boundaries were not considered.

Models of Neuron Polarization Amplification (Principle 2)

For neuron polarization amplification by vasculature, we modeled semi-infinite parallel solid capillaries, adjusting the length density (L_v) of vasculature for varied brain regions (cortical grey-matter, white-matter, subcortical, lumbar white-matter, and lumbar grey-matter; Fig. 2) that are therapeutic targets (Table 1) for different modes of electrical stimulation (tDCS, TMS, ECT, DBS, and SCS). Solid capillaries were modeled with a uniform resistivity of 1×10^5 Ω.m.

Factors driving neuron polarization amplification by vasculature was quantified as normalized electric fields (per unit parenchyma electric field) and normalized activating functions (per unit parenchyma electric field) at three different brain voxel locations: proximal (~ 5 μm away from capillary), middle (in between two capillaries), and distal (no capillary zone) (Fig. 2B1-2B5).

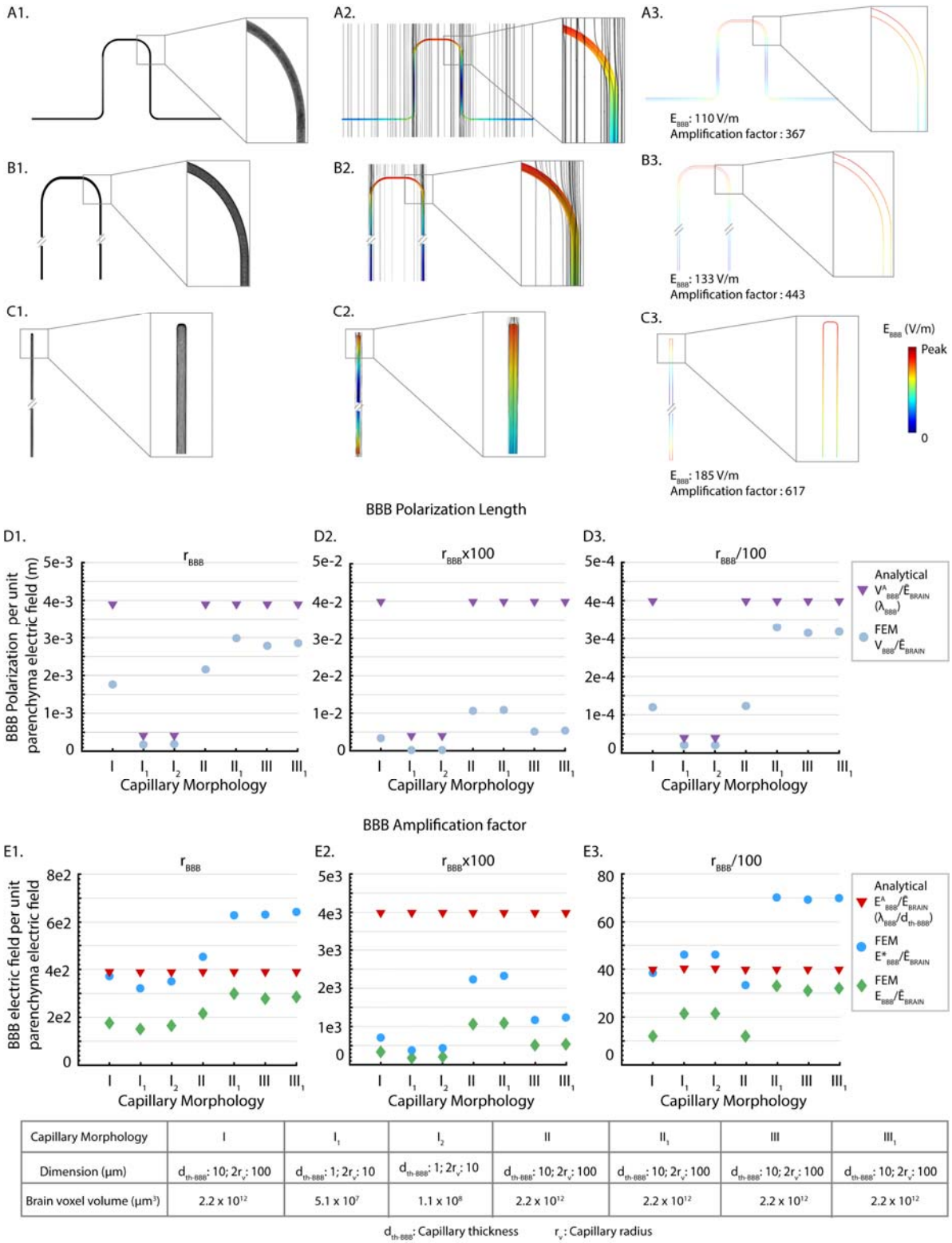

Capillary Morphology	I	I_1	I_2	II	II_1	III	III_1
Dimension (μm)	$d_{th\text{-}BBB}$: 10; $2r_v$: 100	$d_{th\text{-}BBB}$: 1; $2r_v$: 10	$d_{th\text{-}BBB}$: 1; $2r_v$: 10	$d_{th\text{-}BBB}$: 10; $2r_v$: 100	$d_{th\text{-}BBB}$: 10; $2r_v$: 100	$d_{th\text{-}BBB}$: 10; $2r_v$: 100	$d_{th\text{-}BBB}$: 10; $2r_v$: 100
Brain voxel volume (μm^3)	2.2×10^{12}	5.1×10^{7}	1.1×10^{8}	2.2×10^{12}	2.2×10^{12}	2.2×10^{12}	2.2×10^{12}

$d_{th\text{-}BBB}$: Capillary thickness r_v: Capillary radius

Figure 1: Maximal BBB polarization and electric field amplification across prototypical capillary morphologies compared to analytical maxima. Architecture of three exemplary capillary morphologies (A1) Capillary morphology 1: semi-circular loop (fixed curvature width) with semi-infinite orthogonal straight segments, (B1) Capillary morphology 2: semi-circular loop (varied curvatures) with semi-infinite parallel straight segments, and (C1) Capillary morphology 3: semi-infinite straight tube with tapered end.

$d_{th\text{-}BBB}$ and $2r_v$ refers to capillary wall thickness and capillary lumen diameter, respectively. Current flow and specifically maximal electric field intensity across the BBB (E_{BBB}) was predicted. Capillary morphology 1 include three morphological variations (I, I_1, and I_2) with fixed curvature width, but varied $d_{th\text{-}BBB}$ (I: 10 µm; I_1: 1 µm; I_2: 1 µm) and $2r_v$ (I: 100 µm; I_1: 10 µm; I_2: 10 µm). Capillary morphology 2 includes two morphological variations (II and II_1) with similar $d_{th\text{-}BBB}$ (10 µm), $2r_v$ (100 µm) but varied curvature width (II: 1000 µm; II_1: 200 µm). Capillary morphology 3 includes two morphological variations (III and III_1) with similar $d_{th\text{-}BBB}$ (10 µm), $2r_v$ (100 µm), but varied terminal conditions (III: one end open; III_1: both ends sealed). Predicted brain current flow pattern (black flux lines) and BBB electric field (false color) are showed for capillary morphology 1, parameters I (A2, A3), capillary morphology 2, parameters II (B2, B3), and capillary morphology 3, parameters III (C2, C3). The amplification factor (maximal E_{BBB} per unit parenchyma electric field) were 367, 443, and 617, respectively for these three exemplary BBB capillary morphologies and parameters (A3; B3; C3). In addition, for each capillary morphology and variation, BBB resistivity (and so BBB space constant) was varied from a standard value (D1, E1; $r_{BBB} = 1 \times 10^5$ Ω.m) by a factor of 100 up (D2; E2; $r_{BBB}x100 = 1 \times 10^7$ Ω.m) or down (D3; E3; $r_{BBB}/100 = 1 \times 10^3$ Ω.m). For each FEM simulation, BBB polarization per unit brain parenchyma (BBB polarization length) and E_{BBB} per unit brain parenchyma (BBB Amplification factor) is summarized. Since E_{BBB} was not uniform across the vascular wall, we report "punctate" E^*_{BBB} (at any point within the capillary wall) as well as the average E_{BBB} (V_{BBB} / $d_{th\text{-}BBB}$). Finally, the analytically derived (see Methods) maximum BBB polarization length (λ_{BBB}) and BBB Amplification factor ($\lambda_{BBB}/d_{th\text{-}BBB}$) is reported for each model.

Results

Theoretical Basis for Maximum Electric Field Amplification at the BBB (Principle 1)

To develop a theory quantifying BBB (vascular wall) polarization, resulting from current flow between the brain parenchyma and the blood during neuromodulation, we modeled stimulation across capillary segments of varied morphologies that are intended to capture maximum local polarization across a complex capillary network. We considered three prototypical capillary morphologies (Fig. 1 A1, B1, C1). Capillary morphology 1 was a semi-circular loop (fixed curvature width) with semi-infinite orthogonal straight segments, with variants of capillary size (I, I_1, and I_2). Capillary morphology 2 was a semi-circular loop (varied curvatures) with semi-infinite parallel straight segments with variants of loop curvature (II and II_1). Capillary morphology 3 was a semi-infinite straight tube with two variants of terminal conditions (III, III_1). FEM simulation predicted current flow though the brain voxel containing the capillary (Fig. 1 A2, B2, C2), and specifically current flow across the BBB (Fig. 1 A3, B3, C3). Models were designed so that maximum polarization was insensitive to the modeled tissue boundary size (see Methods).

For each morphology, the maximum voltage across the BBB (V_{BBB}) and electric field across the BBB (E_{BBB}) are reported as normalized to unit parenchyma electric field (E_{BRAIN}). This allows reporting of BBB polarization length (V_{BBB} per unit E_{BRAIN}; Fig. 1, row D) and the BBB amplification factor (E_{BBB} per unit E_{BRAIN}; Fig. 1, row E). Thus, for any specific neuromodulation technology with a given average electric field in a brain target, the resulting BBB electric field is this average electric field times the region-specific amplification factor. Finally, for each capillary morphology, BBB resistivity was varied from a standard value (r_{BBB}: Fig. 1D1, 1E1) up or down by a factor of 100 ($r_{BBB}x100$: Fig. 1D2, 1E2; $r_{BBB}/100$: Fig. 1D3, 1E3).

Note that the voltages (V_{BBB}) and electric fields (E_{BBB}) across the BBB segments varied for any capillary morphology; consistent with the objective of this section, we report local maxima for each stimulation. For example, peak E_{BBB} for the exemplary capillary morphologies I, II, and III (with standard r_{BBB}) were, per unit $\tilde{E}_{BRAIN}$: 367 V/m per V/m at capillary bend, 443 V/m per V/m at capillary bend, and 617 V/m per V/m at capillary terminal, respectively (Fig.1A3, 1B3, 1C3). We further predicted a varied electric field across the capillary wall thickness (i.e. the electric field

changes across the BBB wall thickness). Unless otherwise stated, E_{BBB} is considered the average electric field across the capillary wall thickness for a given capillary segment, which is calculated using equation (3). In this section only, we also report the maximal "punctate" electric field across any point inside the capillary wall as E^*_{BBB}.

Based on cable theory (see Methods), we developed an analytical solution for maximum BBB polarization (V^A_{BBB}) which depends only on the space constant (λ_{BBB}) of the vasculature (equation 7). When V^A_{BBB} is expressed per unit $\bar{E}_{BRAIN}$, then the analytical maximum polarization length is simply λ_{BBB}. The analytical solution for maximum BBB electric field (E^A_{BBB}) is then:

$$E^A_{BBB} = \bar{E}_{BRAIN} \times \lambda_{BBB} / d_{th\text{-}BBB} \quad (11)$$

Thus, the analytical maximum electric field amplification factor is $\lambda_{BBB} / d_{th\text{-}BBB}$.

For all the numerically (FEM) simulated capillary parameter, we also predicted (Fig. 1E, 1D) the corresponding analytical maximal BBB voltage (V^A_{BBB}) and electric field (E^A_{BBB}). λ_{BBB} depend on the square root of r_{BBB} (equation 8), as a result, V^A_{BBB} and so $E^A_{BBB,}$ vary by 10x across 100x changes in r_{BBB}. Note analytical predictions do not explicitly depend on capillary morphology (e.g. morphology 1, 2, or 3) but depend on BBB capillary wall and lumen properties. The I_1 and I_2 variations of capillary morphology 1 are thus the only models with different $V^A_{BBB.}$ However, this difference is then absent for predicted E^A_{BBB} because of additional dependence on $d_{th\text{-}BBB}$ (equation 11).

In sum, across different variations of capillary morphologies and BBB capillary wall resistivities, we made two types of comparisons. First, for BBB polarization per unit parenchyma electric field, we compared numerical maxima (V_{BBB} per $\bar{E}_{BRAIN}$) with the analytical BBB polarization (V^A_{BBB} per $\bar{E}_{BRAIN}$) based on λ_{BBB} (Fig. 1, row D). Second, for the BBB electric field amplification (BBB electric field per unit parenchyma electric field) we compared numerically-computed average (E_{BBB} per $\bar{E}_{BRAIN}$) and punctate (E^*_{BBB} per $\bar{E}_{BRAIN}$) BBB electric field amplification with the analytical BBB electric field amplification (E^A_{BBB} per $\bar{E}_{BRAIN}$) based on $\lambda_{BBB} / d_{th\text{-}BBB}$ (Fig. 1, row E).

Across all simulated conditions, the numerically computed maximum polarization length (V_{BBB} per $\bar{E}_{BRAIN}$) was less than the analytical maxima (λ_{BBB}). As a consequence, the numerically computed maximum average BBB electric field (E_{BBB} per $\bar{E}_{BRAIN}$) was also always less than the analytical maximum ($\lambda_{BBB} / d_{th\text{-}BBB}$). In some models, the within-wall numerical maximum BBB electric field (E^*_{BBB} per $\bar{E}_{BRAIN}$) exceed the analytical maximum, but never by more than by a factor of two. Provided our assumptions, the analytical solution for maximum BBB polarization (equation 7) and amplification factor (equation 10) can thus be considered reasonable approximations.

Finally, note that for Principle 1 analysis, an average ("bulk") $\bar{E}_{BRAIN}$ was assumed, however distortion in electric field around the periphery of capillaries was already noted in these simulations and was central to the analysis of non-uniform E_{BRAIN} for Principle 2.

Electric Fields Amplification at the BBB across Neuromodulation Interventions (Principle 1)

We considered five exemplary brain stimulation techniques (tDCS, TMS, ECT, DBS, and SCS) with associated brain targets (cortical, white-matter, subcortical, lumbar spinal white-matter, and lumbar spinal grey-matter). For each brain region, capillary anatomy (wall thickness: $d_{th\text{-}BBB}$; capillary diameter: $2r_v$; lumen diameter: d_l), and BBB membrane and blood resistivities (r_{BBB} and r_{BLOOD}) were derived from prior literature [23–25,56–62]. These values were used to calculate a representative BBB space constant (λ_{BBB}) for each brain region. Typical brain electric field

produced by each stimulation modality were also derived from literature [63–73]. Finally, using the analytical method for predicting maximal BBB polarization length and BBB electric field amplification factor (Fig. 1), for each brain stimulation technique and associated brain region, the maximal BBB polarization (V_{BBB}) and BBB electric field (E_{BBB}) is predicted (Table 1).

The E^A_{BBB} ranges from ~100 V/m for tDCS of cortex to ~100 kV/m for DBS. We note that variations in dose within each neuromodulation modality (e.g. electrode separation) and which brain region is considered (e.g. distance from electrode) causes E_{BRAIN} to vary. Moreover, E_{BRAIN} (and so E_{BBB}) for any modality will vary linearly with applied current. Never-the-less, E^A_{BBB} is consistently greater by over two orders of magnitude than $\bar{E}_{BRAIN}$. The temporal waveform of E_{BBB} would vary for each modality and programming as these setting effect E_{BRAIN}. For example, E_{BBB} would be static for tDCS and would biophysically be pulse for other modalities. Our model assumes no temporal filtering (e.g. low pass) in the BBB amplification factor.

Brain Region	Therapy mode	Capillary thickness (m)	r_{BBB}: $\rho_{BBB}*d_{th\text{-}BBB}/(2\pi r_v)$ (Ω.m)	r_{BLOOD}: $\rho_{BBB}/(\pi d_l^2/4)$ (Ω.m)	λ_{BBB}: $(r_{BBB}/r_{BLOOD})^{1/2}$ (m) [40–42]	Average Electric Field in Brain ROI $\bar{E}_{BRAIN}$ (V/m)	V^A_{BBB}: $\bar{E}_{BRAIN} * \lambda$ (V)	E^A_{BBB}: $V_{BBB}/d_{th\text{-}BBB}$ (V/m)
Cortical	tDCS	1×10^{-6}	4.92×10^{3}	6.08×10^{3}	2.84×10^{-4}	0.3 - 0.6 [63,64]	8.53×10^{-5} - 1.71×10^{-4}	85 -171
Cortical	TMS	1×10^{-6}	4.92×10^{3}	6.08×10^{3}	2.84×10^{-4}	56.5-157.7 [66,67,74]	1.61×10^{-2} - 4.49×10^{-2}	1.61×10^{4} – 4.49×10^{4}
Cortical	ECT	1×10^{-6}	4.92×10^{3}	6.08×10^{3}	2.84×10^{-4}	125-240 [67–69]	3.56×10^{-2} - 6.83×10^{-2}	3.56×10^{4} – 6.83×10^{4}
Subcortical	ECT	1×10^{-6}	4.92×10^{3}	6.28×10^{3}	2.82×10^{-4}	100-125 [68,70]	2.82×10^{-2} - 3.52×10^{-2}	2.82×10^{4} – 3.52×10^{4}
STN, GPi, Thalamus	DBS	1×10^{-6}	4.99×10^{3}	6.57×10^{3}	2.78×10^{-4}	200-1069 [62,71–73]	5.60×10^{-2} - 2.97×10^{-1}	5.56×10^{4} - 2.97×10^{5}
White-matter	SCS	1×10^{-6}	5.08×10^{3}	2.70×10^{-4}	2.70×10^{-4}	14.7-25.6 [60,61]	3.97×10^{-3} - 6.91×10^{-3}	3.97×10^{3} – 6.91×10^{3}
Grey-matter	SCS	1×10^{-6}	5.31×10^{3}	7.28×10^{3}	2.70×10^{-4}	42 [61]	1.13×10^{-2} - 1.49×10^{-2}	1.13×10^{4} –1.49×10^{4}

Table 1: Predicted maximal V_{BBB} and E_{BBB} for various therapeutic modalities and brain targets. Region specific capillary anatomies and resistivities were used to calculate a representative BBB space constant (λ_{BBB}) for each region. Based on our analytical derivation, maximum voltage across the BBB (V^A_{BBB}) and electric field across the BBB (E^A_{BBB}) is calculated.

Theoretical Basis for Neuron Polarization Amplification by Vascular Ultra-structure (Principle 2)

We developed a theory to predict distortion of current flow in the brain parenchyma by capillary ultrastructure and implications for maximum neuronal polarization. For cortical, white-matter, subcortical, lumbar spinal white-matter, and lumbar spinal grey-matter, we derived capillary bed length density (L_v), surface density (S_v), volumetric density (V_v), numerical density (N_v), and intercapillary distance (ICD) (Table 2). A representative vascular network of parallel solid capillaries was modeled for each brain region (Fig. 3, column A). The model was designed to be independent of brain voxel dimension and provide a conservative (uniform, no tortuosity) capillary distribution (see Methods).

For each BBB geometry, the parenchyma electric field (E_{BRAIN}) and electric field gradient (Activating Function) were calculated along three straight trajectories: Proximal (~5 µm away from a capillary at a nearest point), Middle (centered between adjacent capillaries, half the inter-capillary distance at a nearest point), and Distal (no capillary zone, ~100 µm from a capillary at a nearest point). E_{BRAIN} and Activating Function were reported (normalized to) per average parenchyma electric field ($\bar{E}_{BRAIN}$).

Electrical field in the brain parenchyma (E_{BRAIN}) was distorted around brain vasculature, producing ~50% modulation of the average parenchyma electric field ($\bar{E}_{BRAIN}$) (Fig. 2, column B, column C). This change occurs within less than half of an inter-capillary distance, producing Activating Functions of ~100 kV/m^2 per unit average parenchyma electric field ($\bar{E}_{BRAIN}$) (Fig. 2, column D). Both the depth of E_{BRAIN} modulation and spatial rate of change increased with capillary density.

Brain Regions	Therapeutic mode	Length density (L_v: mm/mm^3)	Surface density (S_v: mm^2/mm^3)	Volumetric density (V_v: mm^3/mm^3)	Numerical density (N_v: mm^{-3})	Intercapillary distance (ICD: µm)[75,76]
Cortical	tDCS, TMS, ECT	256 [77]	7.9	0.02	492	45
White-matter	TMS, ECT, DBS	160 [78]	4.9	0.01	307	57
Subcortical	ECT, DBS	328 [48,75,79]	10.1	0.03	631	40
Lumbar White-matter	SCS	810 [80]	24.9	0.06	1558	25
Lumbar Grey-matter	SCS	972 [80]	29.9	0.07	1869	23

Table 2: Vasculature network parameters of different brain region for various therapeutic mode of electrical stimulation.

Neuronal Stimulation Driven by BBB Ultra-structure across Neuromodulation Interventions (Principle 2).

We considered five exemplary brain stimulation techniques (tDCS, TMS, ECT, DBS, and SCS) with associated brain targets (cortical, white-matter, subcortical, lumbar spinal white-matter, and lumbar spinal grey-matter). For each region, relevant capillary anatomy (Table 2) was used to calculate modulated E_{BRAIN} (the range of E_{BRAIN} changes) and Activating Function per unit average parenchyma electric field ($\bar{E}_{BRAIN}$). Next, we combined these constants with specific brain electric fields (Table 3). This analysis assumes negligible "macroscopic" change in E_{BRAIN} across brain voxel in the absence of vasculature (i.e. the electric field is uniform for a homogenous brain voxel) such that any local changes in E_{BRAIN} and non-zero Activating Function are introduced by the presence of vasculature. However, it is the macroscopic changes that are conventionally assumed to drive neuronal stimulation for many modalities. We thus, contrasted Activating Functions generated by conventional macroscopic tissue changes (values derived from literature; [35,61,67,68,70,73,81–85]) with the BBB ultra-structure generated Activating Function derived here. This comparison is subject to a range of assumptions (e.g. distance from electrodes) and simplifications (e.g. linear and homogenous capillary structure). Never-the-less, BBB ultra-structure driven changes may conservatively exceed those conventionally derived from macroscopic tissue changes (Table 3). Moreover, for some techniques, such as tDCS, the electric field is conventionally assumed uniform [35,38] (zero Activating Function), but our analysis instead suggest that it is non-uniform because of spatial modulation by BBB ultra-structure.

Brain Region	Therapy mode	Average Electric Field in Brain ROI $\bar{E}_{BRAIN}$ (V/m)	E_{BRAIN} Modulation from Vascular Ultrastructure (V/m)	Neurovascular Activating Function (Vascular Ultrastructure) (V/m^2)	Conventional Activating Function (Macroscopic) (V/m^2)
Cortical	tDCS	0.3 - 0.6 [63,64]	0.15 – 0.3	1.10×10^4 – 2.21×10^4	0 ([35,81])
Cortical	TMS	56.5-157.7 [66,67,74]	28.3 – 78.9	6.23×10^5 – 5.80×10^6	0 ([67,70])
Cortical	ECT	125-240 [67–69]	62.5 - 120	4.60×10^6 – 8.82×10^6	0 ([68,85])
Subcortical	ECT	100-125 [68,70]	50 – 62.5	3.35×10^6 – 4.19×10^6	0 ([68,85])

STN, GPi, Thalamus	DBS	200-1069 [62,71–73]	100 – 534.5	$6.70x10^{6}$ – $3.58x10^{7}$	$2.2\ x10^{5}$ ([73,82])
White- matter	SCS	14.7-25.6 [60,61]	7.4 – 12.8	$3.74x10^{5}$ – $6.52x10^{5}$	$4.70x10^{4}$ ([61,83])
Grey-matter	SCS	42 [61]	21	$1.85x10^{6}$	$8.14x10^{3}$ ([61,83])

Table 3: Electric field modulation and Activating Function created by BBB ultra-structure for exemplary neuromodulation techniques and brain targets. E_{BRAIN} modulation and Activating functions are reported for the proximal neuronal trajectory.

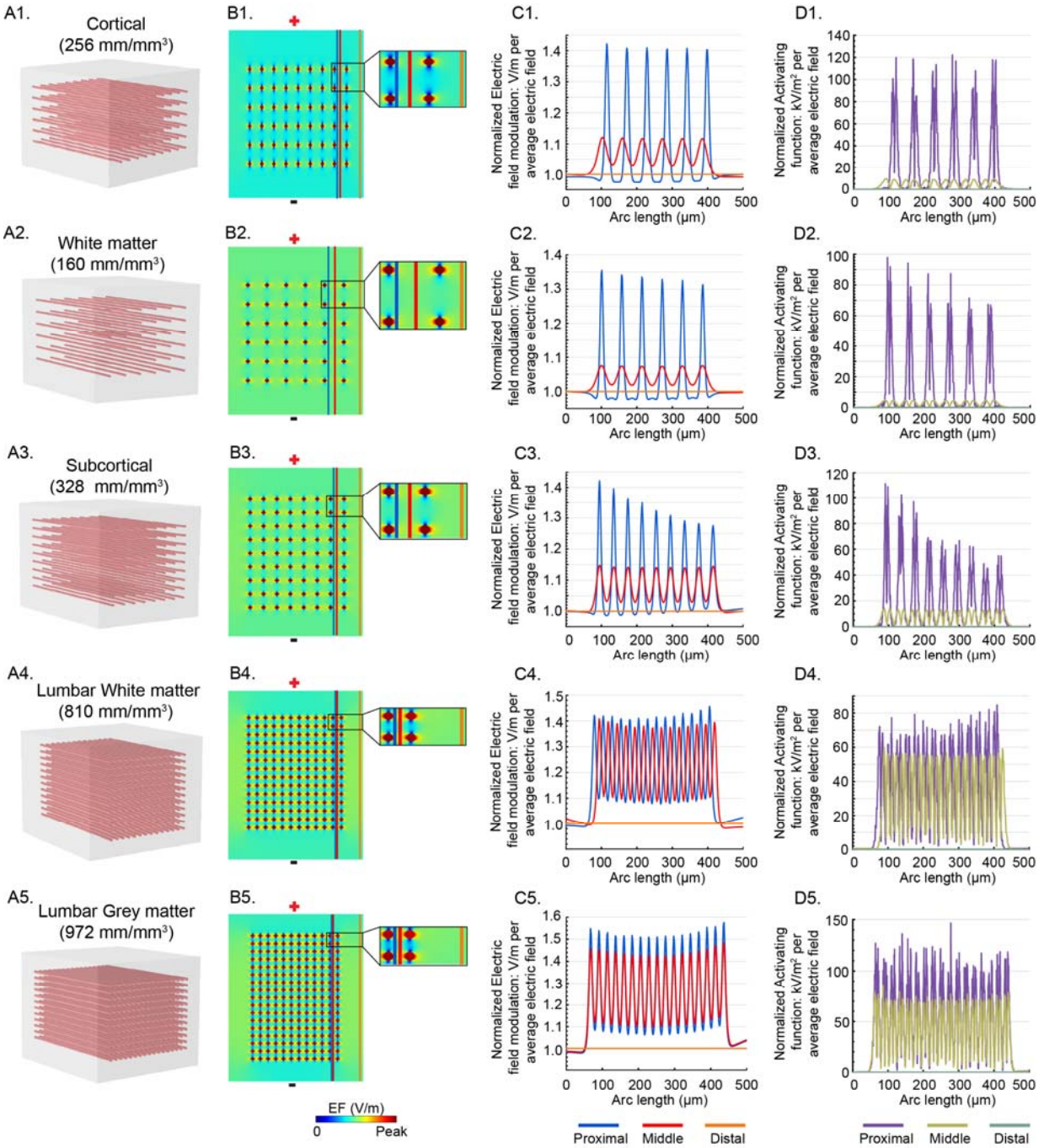

Figure 2: Impact of vascular ultrastructure on brain electric field. We consider vascular ultra-structure network for five brain regions (cortical, white-matter, subcortical, lumbar white-matter, and lumbar grey-matter). (A1, A2, A3, A4, A5) illustrates vascular network for these brain regions, noting the regional capillary length density (mm length per mm^3 volume). (B1, B2, B3, B4, B5) Predicted electric field in a plane crossing the vascular bed, shows local distortion of electric field by the vasculature. Also illustrated is the straight trajectory for sampling of electric field and activating function: 1) Proximal trajectory (~ 5 µm away from nearest capillary; blue line), Middle trajectory (in between adjacent capillaries; red line), and Distal trajectory (region without capillary; orange line).(C1, C2, C3, C4, C5) Normalized electric field magnitude (per unit parenchyma electric field) along three trajectories. The degree of electric field modulation was higher for trajectories passing nearer capillaries and for denser capillary beds. (D1, D2, D3, D4, D5) Electric field gradient (Activating Function) magnitude (per unit parenchyma electric field) along three trajectories. Neuronal activation at the proximity of a vasculature was ~100 kV/m^2 per unit average parenchyma electric field ($\bar{E}_{BRAIN}$). Activating functions were higher for trajectories passing nearer capillaries and for denser capillary beds.

Discussion

The study of which neural elements are activated by neuromodulation is exhaustive and includes verification in isolated systems without vasculature [86–88]. The first principle of neurovascular -modulation, that primary stimulation of BBB function leads to secondary changes in neuronal activity, is complimentary to these conventional theories of direct neural stimulation. We predict the maximal electric field across the BBB (E_{BBB}) are over two orders of magnitude above brain parenchyma (E_{BRAIN}), with a maximum amplification factor ($\lambda_{BBB}/d_{th\text{-}BBB}$) adapted from the cable theory. Electric field across the BBB modulate water and solute transport [20–22] which in turn regulate neuronal metabolic capacity and interstitial clearance. Brain imaging techniques that depend on hemodynamic changes are a bedrock of systems neuroscience (e.g. fMRI, fNIRS) – we suggest that in the specific case of neuromodulation they can be interpreted as suggestive of direct vascular modulation (first principle) rather than secondary neurovascular coupling.

Brain hemodynamics (neurovascular coupling) and BBB transport are disrupted in brain disease, including Alzheimer's Disease and Parkinson's [89–91] and following brain injury [7,92,93]. Indeed, BBB dysfunction may be a link across these disorders [94,95]. Notably, while Alzheimer's disease is traditionally considered a disease of neurofibrillary tangles and amyloid plaques, structural and functional changes in the microvessels may contribute directly to the pathogenesis of the disease [96–100], specifically disruption of brain clearance systems dependent on (water) transport across the BBB [29,101,102]. For a wide range of brain disorders, there is interest in interventions modulating brain hemodynamics and clearance system; neuromodulation may have powerful and unique actions (Principle 1).

When neuromodulation drives intense neuronal activity or relies on neuroplasticity, then neuromodulation is governed by brain metabolism, and so by neurovascular dynamics. The direct stimulation of the BBB by neuromodulation (Principle 1) may thus also play a role in modulating metabolically active states created by direct neuronal stimulation mechanisms. To the extent hemodynamic based functional imaging of neuromodulation does not reflect direct BBB stimulation (Principle 1) but rather conventional neurovascular coupling, it still reinforces the role of the BBB in governing neuronal responses.

The second principle of neurovascular-modulation address direct neural stimulation but with efficacy that is governed by current flow distortion around vascular ultra-structure. We develop a theory relating capillary density to local fluctuations in E_{BBB}. Stimulation of neurons is traditionally modeled as reflecting two cases: 1) changes in E_{BRAIN} along the neural structure

(Activating Function; [44,103,104] or 2) polarization by locally uniform E_{BRAIN} [40,55,105]. In the first case, E_{BRAIN} gradients are conventionally assumed to reflect macroscopic variation in both tissue resistivity and decay with distance from electrodes. However, by Principle 2, local E_{BRAIN} gradients produced by BBB ultra-structure may overwhelm those changes driven by traditional macroscopic models (Table 3). In the second case, Principe 2 suggest locally uniform brain electric fields may in fact not exist. In both cases, that stimulation dose and macro-tissue properties still govern the "incident" E_{BRAIN} arriving at each brain target (modeled here as the average parenchyma electric field ($\bar{E}_{BRAIN}$)), which is then modulated by regional BBB ultra-structure. In this sense, the quasi-uniform assumption remains valid [38,39,106].

These neurovascular-modulation principles are unrelated to BBB injury by electrical stimulation which depends on electrochemical products [107,108]. Activation of neurogenic regulation of cardiac function [109–111] or brain clearance [112] including electrical stimulation of perivascular innervation [113] is distinct from the direct BBB polarization of Principle 2. Electrical stimulation of glia [114–116] and subsequent astrocyte regulation of the BBB [117] are also parallel but distinct pathways.

The capillary bed of the brain is comprised of a dense network of intercommunicating vessels formed by specialized endothelial cells. Endothelial cells and pericytes are encased by basal lamina (~30 – 40 nm thick) containing collagen type IV, heparin sulfate proteoglycans, laminin, fibronectin, and other extracellular matrix proteins [118]. The basal lamina of the brain endothelium is continuous with astrocytic end-feet that ensheath the cerebral capillaries [119,120]. None of these details were modeled here and point to still more intricate mechanisms of neurovascular-modulation.

References

[1] Perlmutter J S, Mink J W, Bastian A J, Zackowski K, Hershey T, Miyawaki E, Koller W and Videen T O 2002 Blood flow responses to deep brain stimulation of thalamus *Neurology* **58** 1388–94

[2] Lang N, Siebner H R, Ward N S, Lee L, Nitsche M A, Paulus W, Rothwell J C, Lemon R N and Frackowiak R S 2005 How does transcranial DC stimulation of the primary motor cortex alter regional neuronal activity in the human brain? *Eur. J. Neurosci.* **22** 495–504

[3] Zheng X, Alsop D C and Schlaug G 2011 Effects of transcranial direct current stimulation (tDCS) on human regional cerebral blood flow *NeuroImage* **58** 26–33

[4] Perrin J S, Merz S, Bennett D M, Currie J, Steele D J, Reid I C and Schwarzbauer C 2012 Electroconvulsive therapy reduces frontal cortical connectivity in severe depressive disorder *Proc. Natl. Acad. Sci. U. S. A.* **109** 5464–8

[5] Ceballos-Baumann A O 2003 Functional imaging in Parkinson's disease: activation studies with PET, fMRI and SPECT *J. Neurol.* **250 Suppl 1** I15-23

[6] Dougherty D D, Chou T, Corse A K, Arulpragasam A R, Widge A S, Cusin C, Evans K C, Greenberg B D, Haber S N and Deckersbach T 2016 Acute deep brain stimulation changes in regional cerebral blood flow in obsessive-compulsive disorder *J. Neurosurg.* **125** 1087–93

[7] Girouard H and Iadecola C 2006 Neurovascular coupling in the normal brain and in hypertension, stroke, and Alzheimer disease *J. Appl. Physiol. Bethesda Md 1985* **100** 328–35

[8] Hosford P S and Gourine A V 2019 What is the key mediator of the neurovascular coupling response? *Neurosci. Biobehav. Rev.* **96** 174–81

[9] Hewson-Stoate N, Jones M, Martindale J, Berwick J and Mayhew J 2005 Further nonlinearities in neurovascular coupling in rodent barrel cortex *NeuroImage* **24** 565–74

[10] Martin C, Martindale J, Berwick J and Mayhew J 2006 Investigating neural–hemodynamic coupling and the hemodynamic response function in the awake rat *NeuroImage* **32** 33–48

[11] Jones M, Hewson-Stoate N, Martindale J, Redgrave P and Mayhew J 2004 Nonlinear coupling of neural activity and CBF in rodent barrel cortex *NeuroImage* **22** 956–65

[12] Logothetis N K, Pauls J, Augath M, Trinath T and Oeltermann A 2001 Neurophysiological investigation of the basis of the fMRI signal *Nature* **412** 150–7

[13] Cardoso M M B, Sirotin Y B, Lima B, Glushenkova E and Das A 2012 The neuroimaging signal is a linear sum of neurally distinct stimulus- and task-related components *Nat. Neurosci.* **15** 1298–306

[14] Lima B, Cardoso M M B, Sirotin Y B and Das A 2014 Stimulus-Related Neuroimaging in Task-Engaged Subjects Is Best Predicted by Concurrent Spiking *J. Neurosci.* **34** 13878–91

[15] Nielsen A N and Lauritzen M 2001 Coupling and uncoupling of activity-dependent increases of neuronal activity and blood flow in rat somatosensory cortex *J. Physiol.* **533** 773–85

[16] Ngai A C, Jolley M A, D'Ambrosio R, Meno J R and Winn H R 1999 Frequency-dependent changes in cerebral blood flow and evoked potentials during somatosensory stimulation in the rat *Brain Res.* **837** 221–8

[17] Hoffmeyer H W, Enager P, Thomsen K J and Lauritzen M J 2007 Nonlinear Neurovascular Coupling in Rat Sensory Cortex by Activation of Transcallosal Fibers *J. Cereb. Blood Flow Metab.* **27** 575–87

[18] Mathiesen C, Caesar K, Akgören N and Lauritzen M 1998 Modification of activity-dependent increases of cerebral blood flow by excitatory synaptic activity and spikes in rat cerebellar cortex *J. Physiol.* **512** 555–66

[19] Akgören N, Dalgaard P and Lauritzen M 1996 Cerebral blood flow increases evoked by electrical stimulation of rat cerebellar cortex: relation to excitatory synaptic activity and nitric oxide synthesis *Brain Res.* **710** 204–14

[20] Shin D W, Fan J, Luu E, Khalid W, Xia Y, Khadka N, Bikson M and Fu B M 2020 In Vivo Modulation of the Blood-Brain Barrier Permeability by Transcranial Direct Current Stimulation (tDCS) *Ann. Biomed. Eng.* **48** 1256–70

[21] Cancel L M, Arias K, Bikson M and Tarbell J M 2018 Direct current stimulation of endothelial monolayers induces a transient and reversible increase in transport due to the electroosmotic effect *Sci. Rep.* **8** 9265

[22] Lopez-Quintero S V, Datta A, Amaya R, Elwassif M, Bikson M and Tarbell J M 2010 DBS-relevant electric fields increase hydraulic conductivity of in vitro endothelial monolayers *J. Neural Eng.* **7** 16005

[23] Duvernoy H, Delon S and Vannson J L 1983 The vascularization of the human cerebellar cortex *Brain Res. Bull.* **11** 419–80

[24] Nicholson C 2001 Diffusion and related transport mechanisms in brain tissue *Rep. Prog. Phys.* **64** 815–884

[25] Schlageter K E, Molnar P, Lapin G D and Groothuis D R 1999 Microvessel organization and structure in experimental brain tumors: microvessel populations with distinctive structural and functional properties *Microvasc. Res.* **58** 312–28

[26] Wong A D, Ye M, Levy A F, Rothstein J D, Bergles D E and Searson P C 2013 The blood-brain barrier: an engineering perspective *Front. Neuroengineering* **6** 7

[27] Iliff J J, Wang M, Liao Y, Plogg B A, Peng W, Gundersen G A, Benveniste H, Vates G E, Deane R, Goldman S A, Nagelhus E A and Nedergaard M 2012 A paravascular pathway facilitates CSF flow through the brain parenchyma and the clearance of interstitial solutes, including amyloid β *Sci. Transl. Med.* **4** 147ra111

[28] Tarasoff-Conway J M, Carare R O, Osorio R S, Glodzik L, Butler T, Fieremans E, Axel L, Rusinek H, Nicholson C, Zlokovic B V, Frangione B, Blennow K, Ménard J, Zetterberg H, Wisniewski T and de Leon M J 2015 Clearance systems in the brain-implications for Alzheimer disease *Nat. Rev. Neurol.* **11** 457–70

[29] Peng W, Achariyar T M, Li B, Liao Y, Mestre H, Hitomi E, Regan S, Kasper T, Peng S, Ding F, Benveniste H, Nedergaard M and Deane R 2016 Suppression of glymphatic fluid transport in a mouse model of Alzheimer's disease *Neurobiol. Dis.* **93** 215–25

[30] Kress B T, Iliff J J, Xia M, Wang M, Wei H S, Zeppenfeld D, Xie L, Kang H, Xu Q, Liew J A, Plog B A, Ding F, Deane R and Nedergaard M 2014 Impairment of paravascular clearance pathways in the aging brain *Ann. Neurol.* **76** 845–61

[31] Xie L, Kang H, Xu Q, Chen M J, Liao Y, Thiyagarajan M, O'Donnell J, Christensen D J, Nicholson C, Iliff J J, Takano T, Deane R and Nedergaard M 2013 Sleep drives metabolite clearance from the adult brain *Science* **342** 373–7

[32] McIntyre C C, Grill W M, Sherman D L and Thakor N V 2004 Cellular Effects of Deep Brain Stimulation: Model-Based Analysis of Activation and Inhibition *J. Neurophysiol.* **91** 1457–69

[33] Ye H and Steiger A 2015 Neuron matters: electric activation of neuronal tissue is dependent on the interaction between the neuron and the electric field *J. Neuroengineering Rehabil.* **12** 65

[34] McIntyre C C and Grill W M 1999 Excitation of central nervous system neurons by nonuniform electric fields *Biophys. J.* **76** 878–88

[35] Datta A, Bansal V, Diaz J, Patel J, Reato D and Bikson M 2009 Gyri-precise head model of transcranial direct current stimulation: improved spatial focality using a ring electrode versus conventional rectangular pad *Brain Stimulat.* **2** 201–7, 207.e1

[36] Rattay F 1999 The basic mechanism for the electrical stimulation of the nervous system *Neuroscience* **89** 335–46

[37] Holsheimer J 1998 Computer modelling of spinal cord stimulation and its contribution to therapeutic efficacy *Spinal Cord* **36** 531–40

[38] Bikson M, Truong D Q, Mourdoukoutas A P, Aboseria M, Khadka N, Adair D and Rahman A 2015 Modeling sequence and quasi-uniform assumption in computational neurostimulation *Prog. Brain Res.* **222** 1–23

[39] Khadka N, Truong D Q, Williams P, Martin J H and Bikson M 2019 The Quasi-uniform assumption for Spinal Cord Stimulation translational research *J. Neurosci. Methods* **328** 108446

[40] Arlotti M, Rahman A, Minhas P and Bikson M 2012 Axon terminal polarization induced by weak uniform DC electric fields: a modeling study *Conf. Proc. Annu. Int. Conf. IEEE Eng. Med. Biol. Soc. IEEE Eng. Med. Biol. Soc. Annu. Conf.* **2012** 4575–8

[41] Rahman A, Lafon B and Bikson M 2015 Multilevel computational models for predicting the cellular effects of noninvasive brain stimulation *Progress in Brain Research* vol 222 (Elsevier) pp 25–40

[42] Rahman A, Reato D, Arlotti M, Gasca F, Datta A, Parra L C and Bikson M 2013 Cellular effects of acute direct current stimulation: somatic and synaptic terminal effects *J. Physiol.* **591** 2563–78

[43] McNeal D R 1976 Analysis of a model for excitation of myelinated nerve *IEEE Trans. Biomed. Eng.* **23** 329–37

[44] Rattay F 1986 Analysis of models for external stimulation of axons *IEEE Trans. Biomed. Eng.* **33** 974–7

[45] Cassot F, Lauwers F, Fouard C, Prohaska S and Lauwers-Cances V 2006 A Novel Three-Dimensional Computer-Assisted Method for a Quantitative Study of Microvascular Networks of the Human Cerebral Cortex *Microcirculation* **13** 1–18

[46] Zawiliński J, Litwin J A, Nowogrodzka-Zagórska M, Gorczyca J and Miodoński A J 2001 Vascular system of the human spinal cord in the prenatal period: a dye injection and corrosion casting study *Ann. Anat. - Anat. Anz.* **183** 331–40

[47] Mozumder M, Pozo J M, Coelho S, Costantini M, Simpson J, Highley J R, Ince P G and Frangi A F 2019 Quantitative histomorphometry of capillary microstructure in deep white matter *NeuroImage Clin.* **23**

[48] Kreczmanski P, Heinsen H, Mantua V, Woltersdorf F, Masson T, Ulfig N, Schmidt-Kastner R, Korr H, Steinbusch H W M, Hof P R and Schmitz C 2009 Microvessel length density, total length, and length per neuron in five subcortical regions in schizophrenia *Acta Neuropathol. (Berl.)* **117** 409–21

[49] Pienaar I S, Lee C H, Elson J L, McGuinness L, Gentleman S M, Kalaria R N and Dexter D T 2015 Deep-brain stimulation associates with improved microvascular integrity in the subthalamic nucleus in Parkinson's disease *Neurobiol. Dis.* **74** 392–405

[50] Bouras C, Kövari E, Herrmann F R, Rivara C-B, Bailey T L, von Gunten A, Hof P R and Giannakopoulos P 2006 Stereologic analysis of microvascular morphology in the elderly: Alzheimer disease pathology and cognitive status *J. Neuropathol. Exp. Neurol.* **65** 235–44

[51] Marín-Padilla M 2012 The human brain intracerebral microvascular system: development and structure *Front. Neuroanat.* **6** 38

[52] Lauwers F, Cassot F, Lauwers-Cances V, Puwanarajah P and Duvernoy H 2008 Morphometry of the human cerebral cortex microcirculation: general characteristics and space-related profiles *NeuroImage* **39** 936–48

[53] Rubinstein J T 1993 Axon termination conditions for electrical stimulation *IEEE Trans. Biomed. Eng.* **40** 654–63

[54] Chakraborty D, Truong D Q, Bikson M and Kaphzan H 2018 Neuromodulation of Axon Terminals *Cereb. Cortex N. Y. N 1991* **28** 2786–94

[55] Tranchina D and Nicholson C 1986 A model for the polarization of neurons by extrinsically applied electric fields *Biophys. J.* **50** 1139–56

[56] Hasgall P, Gennaro F, Baumgartner C, Neufeld E, Lloyd B, Gosselin M, Payne D, Klingenböck A and Kuster N IT'IS Database for thermal and electromagnetic parameters of biological tissues

[57] Butt A M, Jones H C and Abbott N J 1990 Electrical resistance across the blood-brain barrier in anaesthetized rats: a developmental study *J. Physiol.* **429** 47–62

[58] Srinivasan B, Kolli A R, Esch M B, Abaci H E, Shuler M L and Hickman J J 2015 TEER measurement techniques for in vitro barrier model systems *J. Lab. Autom.* **20** 107–26

[59] Marquez J, van Vliet P, McElduff P, Lagopoulos J and Parsons M 2015 Transcranial Direct Current Stimulation (tDCS): Does it Have Merit in Stroke Rehabilitation? A Systematic Review *Int. J. Stroke* **10** 306–16

[60] Hernández-Labrado G R, Polo J L, López-Dolado E and Collazos-Castro J E 2011 Spinal cord direct current stimulation: finite element analysis of the electric field and current density *Med. Biol. Eng. Comput.* **49** 417–29

[61] Khadka N, Liu X, Zander H, Swami J, Rogers E, Lempka S and Bikson M 2020 Realistic anatomically detailed open-source spinal cord stimulation (RADO-SCS) model *J. Neural Eng.*

[62] Khadka N, Harmsen I E, Lozano A M and Bikson M Bio-Heat Model of Kilohertz-Frequency Deep Brain Stimulation Increases Brain Tissue Temperature *Neuromodulation Technol. Neural Interface* **n/a**

[63] Truong D Q, Magerowski G, Blackburn G L, Bikson M and Alonso-Alonso M 2013 Computational modeling of transcranial direct current stimulation (tDCS) in obesity: Impact of head fat and dose guidelines *NeuroImage Clin.* **2** 759–66

[64] Datta A, Truong D, Minhas P, Parra L C and Bikson M 2012 Inter-Individual Variation during Transcranial Direct Current Stimulation and Normalization of Dose Using MRI-Derived Computational Models *Front. Psychiatry* **3** 91

[65] Mikkonen M, Laakso I, Sumiya M, Koyama S, Hirata A and Tanaka S 2018 TMS Motor Thresholds Correlate With TDCS Electric Field Strengths in Hand Motor Area *Front. Neurosci.* **12**

[66] Janssen A M, Oostendorp T F and Stegeman D F 2015 The coil orientation dependency of the electric field induced by TMS for M1 and other brain areas *J. NeuroEngineering Rehabil.* **12** 47

[67] Deng Z-D, Liston C, Gunning F M, Dubin M J, Fridgeirsson E A, Lilien J, van Wingen G and van Waarde J 2019 Electric Field Modeling for Transcranial Magnetic Stimulation and Electroconvulsive Therapy *Brain and Human Body Modeling: Computational Human Modeling at EMBC 2018* ed S Makarov, M Horner and G Noetscher (Cham: Springer International Publishing) pp 75–84

[68] Bai S, Gálvez V, Dokos S, Martin D, Bikson M and Loo C 2017 Computational models of Bitemporal, Bifrontal and Right Unilateral ECT predict differential stimulation of brain regions associated with efficacy and cognitive side effects *Eur. Psychiatry J. Assoc. Eur. Psychiatr.* **41** 21–9

[69] Argyelan M, Oltedal L, Deng Z-D, Wade B, Bikson M, Joanlanne A, Sanghani S, Bartsch H, Cano M, Dale A M, Dannlowski U, Dols A, Enneking V, Espinoza R, Kessler U, Narr K L, Oedegaard K J, Oudega M L, Redlich R, Stek M L, Takamiya A, Emsell L, Bouckaert F, Sienaert P, Pujol J, Tendolkar I, van Eijndhoven P, Petrides G, Malhotra A K and Abbott C 2019 Electric field causes volumetric changes in the human brain *eLife* **8**

[70] Lee W H, Lisanby S H, Laine A F and Peterchev A V 2016 Comparison of electric field strength and spatial distribution of electroconvulsive therapy and magnetic seizure therapy in a realistic human head model. *Eur. Psychiatry J. Assoc. Eur. Psychiatr.* **36** 55–64

[71] Hemm S, Mennessier G, Vayssiere N, Cif L, Fertit H E and Coubes P 2005 Deep brain stimulation in movement disorders: stereotactic coregistration of two-dimensional electrical field modeling and magnetic resonance imaging *J. Neurosurg.* **103** 949–55

[72] Hemm S, Mennessier G, Vayssière N, Cif L and Coubes P 2005 Co-registration of stereotactic MRI and isofieldlines during deep brain stimulation *Brain Res. Bull.* **68** 59–61

[73] Astrom M, Diczfalusy E, Martens H and Wardell K 2015 Relationship between neural activation and electric field distribution during deep brain stimulation *IEEE Trans. Biomed. Eng.* **62** 664–72

[74] Mikkonen M, Laakso I, Sumiya M, Koyama S, Hirata A and Tanaka S 2018 TMS Motor Thresholds Correlate With TDCS Electric Field Strengths in Hand Motor Area *Front. Neurosci.* **12** 426

[75] Boero J A, Ascher J, Arregui A, Rovainen C and Woolsey T A 1999 Increased brain capillaries in chronic hypoxia *J. Appl. Physiol. Bethesda Md 1985* **86** 1211–9

[76] Dockery P and Fraher J 2007 The quantification of vascular beds: A stereological approach *Exp. Mol. Pathol.* **82** 110–20

[77] Kubíková T, Kochová P, Tomášek P, Witter K and Tonar Z 2018 Numerical and length densities of microvessels in the human brain: Correlation with preferential orientation of microvessels in the cerebral cortex, subcortical grey matter and white matter, pons and cerebellum *J. Chem. Neuroanat.* **88** 22–32

[78] Kaplan S 2018 Non-steroidal anti-inflammatory drugs and nervous system development *J. Chem. Neuroanat.* **87** 1

[79] Acer N, Bastepe-Gray S, Sagiroglu A, Gumus K Z, Degirmencioglu L, Zararsiz G and Ozic M U 2018 Diffusion tensor and volumetric magnetic resonance imaging findings in the brains of professional musicians *J. Chem. Neuroanat.* **88** 33–40

[80] O'Sullivan C, Dockery P and Fraher J P 2004 P2: The vascular anatomy of the human spinal cord *J. Anat.* **205** 528

[81] Jiang J, Truong D Q, Esmaeilpour Z, Huang Y, Badran B W and Bikson M 2020 Enhanced tES and tDCS computational models by meninges emulation *J. Neural Eng.* **17** 016027

[82] Kuncel A M, Cooper S E and Grill W M 2008 A method to estimate the spatial extent of activation in thalamic deep brain stimulation *Clin. Neurophysiol.* **119** 2148–58

[83] Zannou A L, Khadka N, Truong D Q, Zhang T, Esteller R, Hershey B and Bikson M 2019 Temperature increases by kilohertz frequency spinal cord stimulation *Brain Stimulat.* **12** 62–72

[84] Deng Z-D, Lisanby S H and Peterchev A V 2013 Controlling stimulation strength and focality in electroconvulsive therapy via current amplitude and electrode size and spacing: comparison with magnetic seizure therapy *J. ECT* **29** 325–35

[85] Deng Z-D, Lisanby S H and Peterchev A V 2011 Electric field strength and focality in electroconvulsive therapy and magnetic seizure therapy: a finite element simulation study *J. Neural Eng.* **8** 016007

[86] Maccabee P J, Amassian V E, Eberle L P and Cracco R Q 1993 Magnetic coil stimulation of straight and bent amphibian and mammalian peripheral nerve in vitro: locus of excitation *J. Physiol.* **460** 201–19

[87] Bikson M, Inoue M, Akiyama H, Deans J K, Fox J E, Miyakawa H and Jefferys J G R 2004 Effects of uniform extracellular DC electric fields on excitability in rat hippocampal slices in vitro *J. Physiol.* **557** 175–90

[88] Förstl J, Galvan M and ten Bruggencate G 1982 Extracellular K+ concentration during electrical stimulation of rat isolated sympathetic ganglia, vagus and optic nerves *Neuroscience* **7** 3221–9

[89] Grammas P, Martinez J and Miller B 2011 Cerebral microvascular endothelium and the pathogenesis of neurodegenerative diseases *Expert Rev. Mol. Med.* **13** e19

[90] Sweeney M D, Sagare A P and Zlokovic B V 2018 Blood-brain barrier breakdown in Alzheimer disease and other neurodegenerative disorders *Nat. Rev. Neurol.* **14** 133–50

[91] Amtul Z, Yang J, Lee T-Y and Cechetto D F 2019 Pathological Changes in Microvascular Morphology, Density, Size and Responses Following Comorbid Cerebral Injury *Front. Aging Neurosci.* **11** 47

[92] Jang H, Huang S, Hammer D X, Wang L, Rafi H, Ye M, Welle C G and Fisher J A N 2017 Alterations in neurovascular coupling following acute traumatic brain injury *Neurophotonics* **4** 045007

[93] Wright A D, Smirl J D, Bryk K and van Donkelaar P 2017 A Prospective Transcranial Doppler Ultrasound-Based Evaluation of the Acute and Cumulative Effects of Sport-Related Concussion on Neurovascular Coupling Response Dynamics *J. Neurotrauma* **34** 3097–106

[94] Rosengarten B, Dannhardt V, Burr O, Pöhler M, Rosengarten S, Oechsner M and Reuter I 2010 Neurovascular coupling in Parkinson's disease patients: effects of dementia and acetylcholinesterase inhibitor treatment *J. Alzheimers Dis. JAD* **22** 415–21

[95] Abrahamson E E and Ikonomovic M D 2020 Brain injury-induced dysfunction of the blood brain barrier as a risk for dementia *Exp. Neurol.* **328** 113257

[96] Drachman D A 2014 The amyloid hypothesis, time to move on: Amyloid is the downstream result, not cause, of Alzheimer's disease *Alzheimers Dement. J. Alzheimers Assoc.* **10** 372–80

[97] Tarantini S, Tran C H T, Gordon G R, Ungvari Z and Csiszar A 2017 Impaired neurovascular coupling in aging and Alzheimer's disease: Contribution of astrocyte dysfunction and endothelial impairment to cognitive decline *Exp. Gerontol.* **94** 52–8

[98] Liu Y, Braidy N, Poljak A, Chan D K Y and Sachdev P 2018 Cerebral small vessel disease and the risk of Alzheimer's disease: A systematic review *Ageing Res. Rev.* **47** 41–8

[99] Costea L, Mészáros Á, Bauer H, Bauer H-C, Traweger A, Wilhelm I, Farkas A E and Krizbai I A 2019 The Blood-Brain Barrier and Its Intercellular Junctions in Age-Related Brain Disorders *Int. J. Mol. Sci.* **20**

[100] Roquet D, Sourty M, Botzung A, Armspach J-P and Blanc F 2016 Brain perfusion in dementia with Lewy bodies and Alzheimer's disease: an arterial spin labeling MRI study on prodromal and mild dementia stages *Alzheimers Res. Ther.* **8** 29

[101] Anderson V C, Lenar D P, Quinn J F and Rooney W D 2011 The blood-brain barrier and microvascular water exchange in Alzheimer's disease *Cardiovasc. Psychiatry Neurol.* **2011** 615829

[102] van de Haar H J, Burgmans S, Jansen J F A, van Osch M J P, van Buchem M A, Muller M, Hofman P A M, Verhey F R J and Backes W H 2016 Blood-Brain Barrier Leakage in Patients with Early Alzheimer Disease *Radiology* **281** 527–35

[103] Warman E N, Grill W M and Durand D 1992 Modeling the effects of electric fields on nerve fibers: determination of excitation thresholds *IEEE Trans. Biomed. Eng.* **39** 1244–54

[104] McIntyre C C and Grill W M 2002 Extracellular stimulation of central neurons: influence of stimulus waveform and frequency on neuronal output *J. Neurophysiol.* **88** 1592–604

[105] Radman T, Ramos R L, Brumberg J C and Bikson M 2009 Role of cortical cell type and morphology in subthreshold and suprathreshold uniform electric field stimulation in vitro *Brain Stimulat.* **2** 215–28, 228.e1-3

[106] Bikson M, Dmochowski J and Rahman A 2013 The “quasi-uniform” assumption in animal and computational models of non-invasive electrical stimulation *Brain Stimulat.* **6** 704–5

[107] Pudenz R H, Bullara L A, Jacques S and Hambrecht F T 1975 Electrical stimulation of the brain. III. The neural damage model *Surg. Neurol.* **4** 389–400

[108] Fox J L and Yasargil M G 1974 The experimental effect of direct electrical current on intracranial arteries and the blood-brain barrier *J. Neurosurg.* **41** 582–9

[109] ter Laan M, van Dijk J M C, Stewart R, Staal M J and Elting J-W J 2014 Modulation of cerebral blood flow with transcutaneous electrical neurostimulation (TENS) in patients with cerebral vasospasm after subarachnoid hemorrhage *Neuromodulation J. Int. Neuromodulation Soc.* **17** 431–6; discussion 436-437

[110] ter Laan M, van Dijk J M C, Elting J W J, Staal M J and Absalom A R 2013 Sympathetic regulation of cerebral blood flow in humans: a review *Br. J. Anaesth.* **111** 361–7

[111] Bapna A, Adin C, Engelman Z J and Fudim M 2019 Increasing Blood Pressure by Greater Splanchnic Nerve Stimulation: a Feasibility Study *J Cardiovasc. Transl. Res.*

[112] Cheng K P, Brodnick S K, Blanz S L, Zeng W, Kegel J, Pisaniello J A, Ness J P, Ross E, Nicolai E N, Settell M L, Trevathan J K, Poore S O, Suminski A J, Williams J C and Ludwig K A 2020 Clinically-derived vagus nerve stimulation enhances cerebrospinal fluid penetrance *Brain Stimulat.* **13** 1024–30

[113] Suzuki N and Hardebo J E 1993 The cerebrovascular parasympathetic innervation *Cerebrovasc. Brain Metab. Rev.* **5** 33–46

[114] Bikson M, Lian J, Hahn P J, Stacey W C, Sciortino C and Durand D M 2001 Suppression of epileptiform activity by high frequency sinusoidal fields in rat hippocampal slices *J. Physiol.* **531** 181–91

[115] Vallejo R, Platt D C, Rink J A, Jones M A, Kelley C A, Gupta A, Cass C L, Eichenberg K, Vallejo A, Smith W J, Benyamin R and Cedeño D L 2019 Electrical Stimulation of C6 Glia-Precursor Cells In Vitro Differentially Modulates Gene Expression Related to Chronic Pain Pathways *Brain Sci.* **9**

[116] Monai H, Ohkura M, Tanaka M, Oe Y, Konno A, Hirai H, Mikoshiba K, Itohara S, Nakai J, Iwai Y and Hirase H 2016 Calcium imaging reveals glial involvement in transcranial direct current stimulation-induced plasticity in mouse brain *Nat. Commun.* **7** 11100

[117] MacVicar B A and Newman E A 2015 Astrocyte regulation of blood flow in the brain *Cold Spring Harb. Perspect. Biol.* **7**

[118] Thomsen M S, Routhe L J and Moos T 2017 The vascular basement membrane in the healthy and pathological brain *J. Cereb. Blood Flow Metab. Off. J. Int. Soc. Cereb. Blood Flow Metab.* **37** 3300–17

[119] Daneman R and Prat A 2015 The blood-brain barrier *Cold Spring Harb. Perspect. Biol.* **7** a020412

[120] Jessen N A, Munk A S F, Lundgaard I and Nedergaard M 2015 The Glymphatic System: A Beginner's Guide *Neurochem. Res.* **40** 2583–99

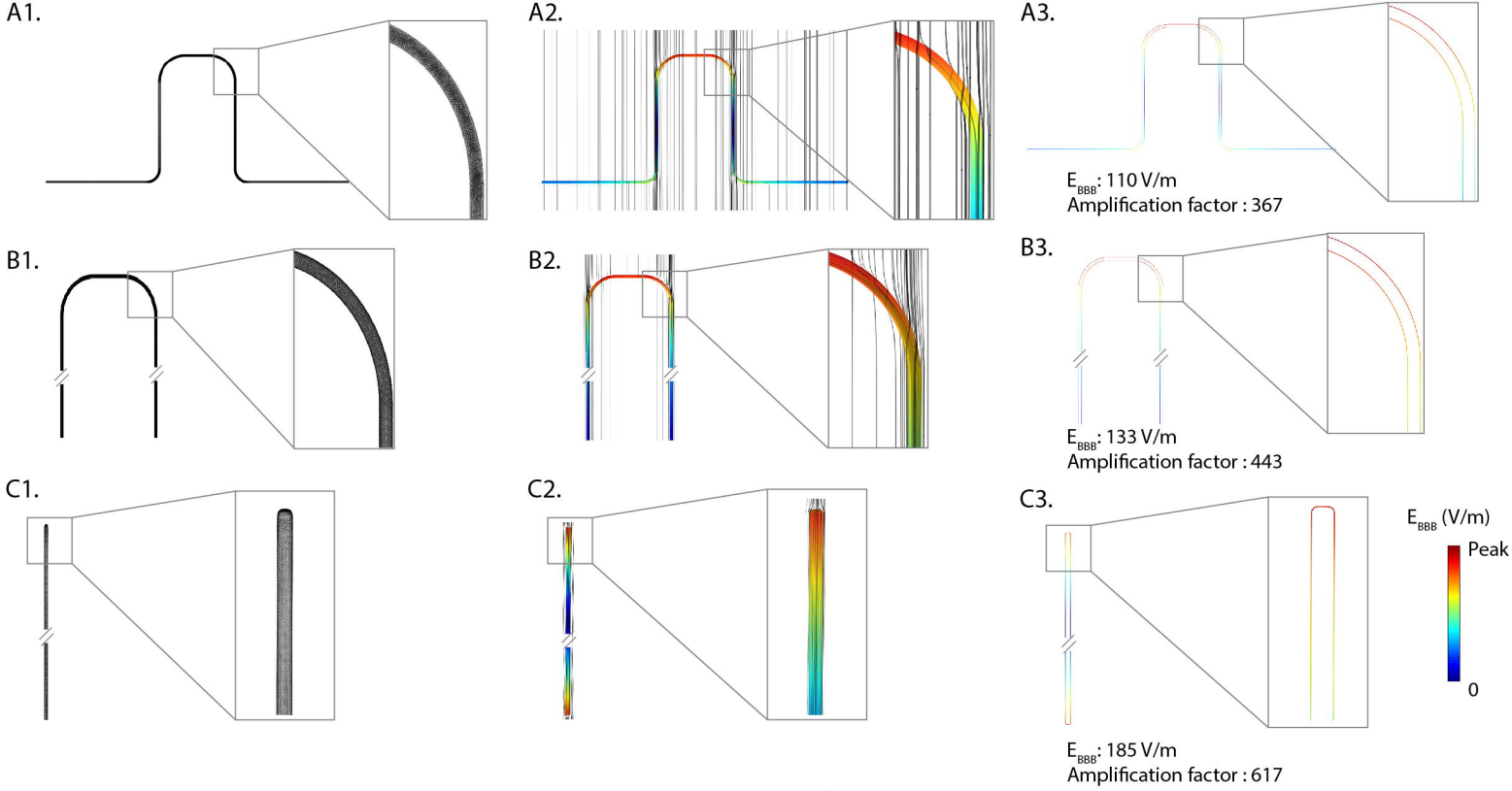

BBB Polarization Length

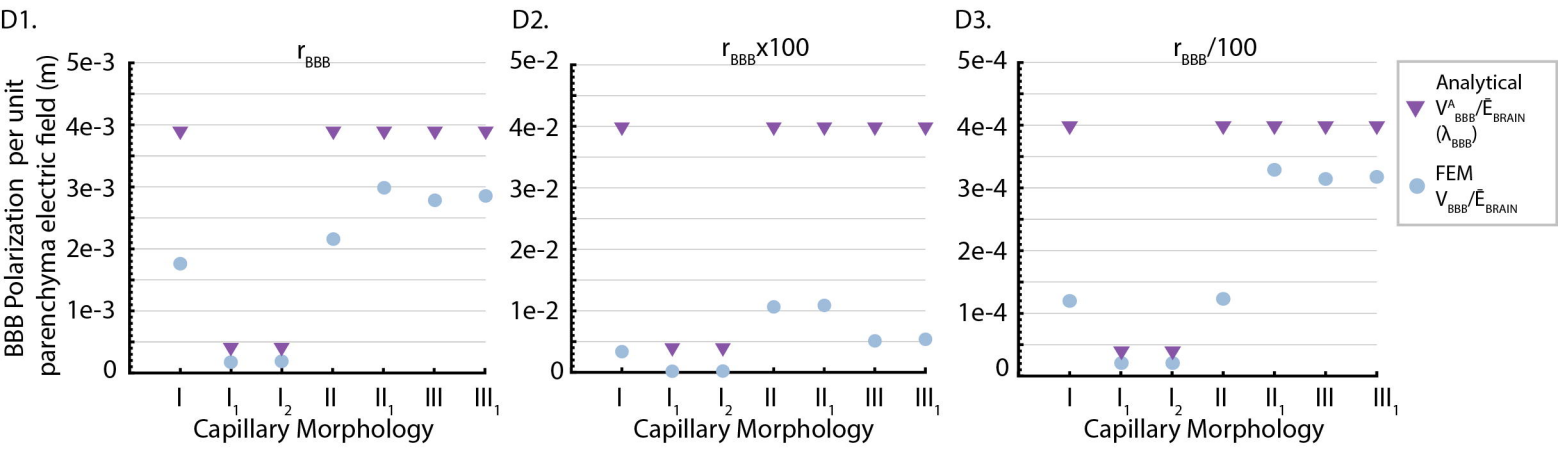

BBB Amplification factor

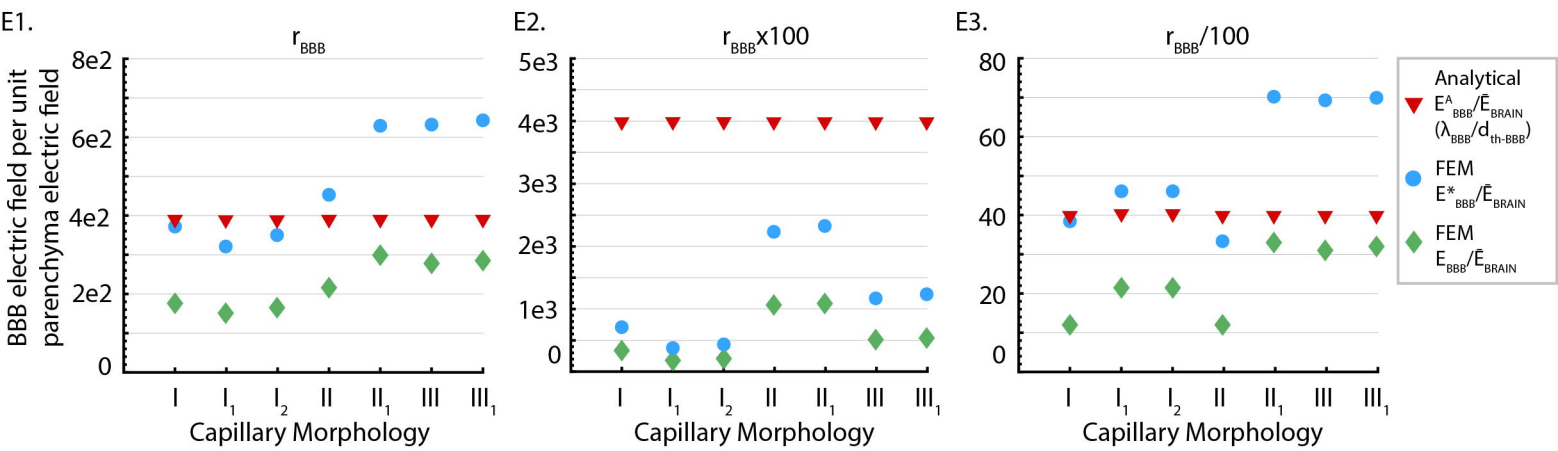

Capillary Morphology	I	I_1	I_2	II	II_1	III	III_1
Dimension (μm)	$d_{th\text{-}BBB}$: 10; $2r_v$: 100	$d_{th\text{-}BBB}$: 1; $2r_v$: 10	$d_{th\text{-}BBB}$: 1; $2r_v$: 10	$d_{th\text{-}BBB}$: 10; $2r_v$: 100	$d_{th\text{-}BBB}$: 10; $2r_v$: 100	$d_{th\text{-}BBB}$: 10; $2r_v$: 100	$d_{th\text{-}BBB}$: 10; $2r_v$: 100
Brain voxel volume (μm^3)	2.2×10^{12}	5.1×10^{7}	1.1×10^{8}	2.2×10^{12}	2.2×10^{12}	2.2×10^{12}	2.2×10^{12}

$d_{th\text{-}BBB}$: Capillary thickness r_v: Capillary radius

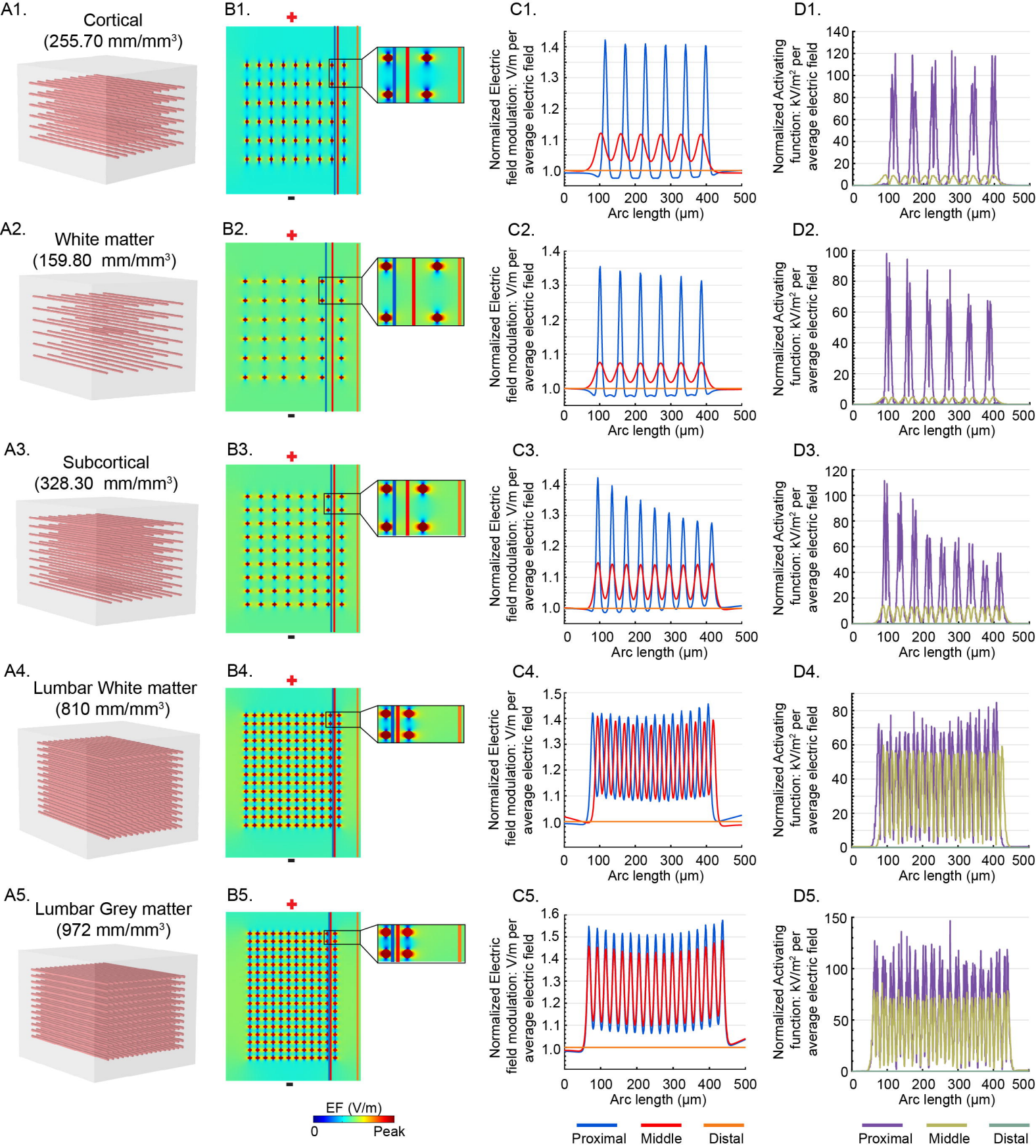
A1.
Cortical
(255.70 mm/mm³)
A2.
White matter
(159.80 mm/mm³)
A3.
Subcortical
(328.30 mm/mm³)
A4.
Lumbar White matter
(810 mm/mm³)
A5.
Lumbar Grey matter
(972 mm/mm³)
B1.
B2.
B3.
B4.
B5.
EF (V/m)
0
Peak
C1.
C2.
C3.
C4.
C5.
Normalized Electric field modulation: V/m per average electric field
Arc length (μm)
D1.
D2.
D3.
D4.
D5.
Normalized Activating function: kV/m² per average electric field
Arc length (μm)
Proximal
Middle
Distal
Proximal
Middle
Distal